Structural and magnetic properties of Ln(III) complexes with diimines and crotonato as a bridging ligand

Ana María Atria [a,*], Ricardo Baggio [b], María Teresa Garland [c], Juan Carlos Muñoz [a], Octavio Peña [d]

[a] *Facultad de Ciencias Químicas y Farmacéuticas and CIMAT, Universidad de Chile, Casilla 233, Santiago, Chile*
[b] *Departamento de Física, Comisión Nacional de Energía Atómica, Avda. del Libertador 8250, Buenos Aires, 1429, Argentina*
[c] *Departamento de Física, Facultad de Ciencias Físicas y Matemáticas and CIMAT, Universidad de Chile, Avda. Blanco Encalada 2008, Casilla 487-3, Santiago, Chile*
[d] *L.C.S.I.M./UMR 6511 CNRS/Institut de Chimie de Rennes, Université de Rennes1, Rennes, France*

Abstract

Five new lanthanide complexes displaying crotonato bridges have been prepared: $[Gd_2(crot)_6(H_2O)_4]\cdot 4(bpa)$ (**1**); $[Ho_2(crot)_7]_n\cdot(Hbpa)$ (**2**); $[Gd_2(crot)_6(bipy)_2]$ (**3**); $[Ho_2(crot)_6(bipy)_2]$ (**4**) and $[Nd_2(crot)_6(H_2O)_3]_n$ (**5**), where bipy = 2,2′-bipyridine; bpa = di(2-pyridyl)amine; crot = crotonato. The compounds were characterized by magnetic susceptibility measurements and their crystal structures were determined by single crystal X-ray diffraction. These studies showed complexes **1**, **3** and **4** to be dimers while structures **2** and **5** are polymeric in nature.

Keywords: Lanthanides complexes; Structures; Magnetism

1. Introduction

In the last few years an increasing interest in the study of the coordination chemistry of lanthanide metal ions has been observed, possibly due to the variety of potential applications of their complexes, mainly in medicine and, specifically, as magnetic resonance contrasting agents [1–5]. In spite of this, little attention has been given to the nature of the magnetic coupling in such species. From this point of view, homonuclear complexes of rare earth metals have been much less extensively studied than their hetero polynuclear counterparts. The scarce magnetic investigations performed on the subject have mostly been focussed on the nature of the Gd(III)–Gd(III) coupling because of their relative simplicity as compared with the well-known complexity involved in the study of the remaining Ln(III) ions, where both orbital as well as crystal field effects have to be considered in the interpretation of results.

In addition to the quality of the magnetic centers, there is an extra factor adding up to the general complexity of the problem as is the type of structural link between them. It is well known that magnetic interactions between paramagnetic centers can take place not only through single atoms but also through multiatomic bridges, as those provided by carboxylato and other O–C–O ligands which are known to be good transmission agents through a variety of bridging conformations, viz, pure bridging bidentate (in $\eta^1\eta^1\mu_2$, in a *syn–syn*, *syn–anti* or *anti–anti* configuration), chelato-bridging tridentate ($\eta^2\eta^1\mu_2$), etc., which, when operating over rare earth centers, usually determine rather complex structures with potentially interesting magnetic properties [6–8].

As a contribution to the understanding of this kind of homonuclear complexes we present herein the synthesis, structural and magnetic characterization of five such new lanthanide (III) compounds complexed to crotonato

* Corresponding author. Fax: +56-2-737-0567, +56-2-737-8920.
E-mail address: aatria@ciq.uchile.cl (A.M. Atria).

anions and diimines, formulated as $[Gd_2(crot)_6(H_2O)_4] \cdot 4(bpa)$ (**1**); $[Ho_2(crot)_7]_n \cdot (Hbpa)$ (**2**); $[Gd_2(crot)_6\ (bipy)_2]$ (**3**); $[Ho_2(crot)_6(bipy)_2]$ (**4**) and $[Nd_2(crot)_6\ (H_2O)_3]_n$ (**5**), where bipy = 2,2′-bipyridine; bpa = di(2-pyridyl)amine; crot = crotonato.

2. Experimental section

2.1. Synthesis

All five complexes were synthesized by similar methods: a mixture of Ln_2O_3 (1 mmol) and crotonic acid (6 mmol) was dissolved in water (100 mmol), followed by the addition of the imine ligand (1 mmol) dissolved in methanol (10 mL). The resultant mixture was refluxed for 24 h, filtered while hot, and then concentrated to 25 mL. The filtrate was left at room temperature. On standing, colorless crystals suitable for single crystal X-ray diffraction appeared, which were used without further processing.

2.2. Crystal structure determination

Highly redundant diffractometer data sets were collected at room temperature ($T = 295$ K) for all three structures, up to a 2θ max. of ca. 58°, with a Bruker AXS SMART APEX CCD diffractometer using monochromatic Mo Kα radiation, $\lambda = 0.71069$ Å, and a 0.3° separation between frames. For each one, data integration was performed using SAINT and a semi-empirical absorption correction was applied using SADABS, both programs being included in the diffractometer package. In all cases, the structure resolution was achieved routinely by direct methods and difference Fourier. The structures were refined by least squares on F^2, with anisotropic displacement parameters for non-H atoms. Structure **2** crystallizes in space group *Cc*, but as a racemic twin of equally populated halves. Inspection for a possible crystallographic centering proved unsuccessful.

In all five structures, hydrogen atoms attached to carbon (C–H) were placed at their calculated positions and allowed to ride onto their host carbons both in coordinates as well as in thermal parameters. Terminal methyl groups were allowed to rotate as well. Hydrogen atoms deemed as potentially active in H-bonding interactions (O–H and N–H) were searched in the late Fouriers, and treated in accordance to the data set qualities. Thus, all of them were located in structure **1** and refined with restrained X–H distances (0.78(1) Å); In structure **2**, only N–H were found, and left free to refine. Those corresponding to the disordered water molecules, instead, could not be located, the same as those in structure **5**, all of which were accordingly disregarded from the models.

All calculations to solve the structures, refine the proposed models and obtain derived results were carried out

Table 1
Crystal and refinement data for structures **1**, **2**, **3**, **4** and **5**

Compound	GdBPA (**1**)	HoBPA (**2**)	GdBiPY (**3**)	HoBiPY (**4**)	NdCrot (**5**)
Formula	$C_{64}H_{74}Gd_2N_{12}O_{16}$	$C_{38}H_{49}Ho_2N_3O_{16}$	$C_{44}H_{46}Gd_2N_4O_{12}$	$C_{44}H_{46}Ho_2N_4O_{12}$	$C_{24}H_{44}Nd_2O_{19}$
Formula weight	1581.85	1133.66	1137.35	1152.70	925.07
Crystal system	monoclinic	monoclinic	triclinic	triclinic	monoclinic
Space group	$C2/c$ (no. 15)	Cc (no. 9)	$P\bar{1}$ (no. 2)	$P\bar{1}$ (no. 2)	$P2_1/c$ (no. 14)
Crystal shape, color	blocks pale rose	blocks colorless	blocks pale rose	blocks colorless	blocks pale violet
a (Å)	38.243(3)	19.395(3)	10.106(1)	10.120(3)	11.962(2)
b (Å)	8.917(1)	17.142(2)	10.579(1)	10.586(3)	14.193(2)
c (Å)	25.670(2)	15.814(2)	11.296(1)	11.283(3)	22.174(4)
α (°)	90	90	70.72(1)	70.97(1)	90
β (°)	126.63(1)	118.91(1)	73.82(1)	73.57(1)	101.08(1)
γ (°)	90	90	80.83(1)	80.71(1)	90
V (Å^3)	7025.2(8)	4602.6(11)	1091.7(2)	1092.8(5)	3694.5(10)
Z	4	4	1	1	4
$d_{calc.}$ (g cm^{-3})	1.50	1.64	1.73	1.75	1.66
$F(000)$	3192	2240	562	568	1840
μ (mm^{-1})	1.94	3.48	3.08	3.66	2.85
θ range	1.98–27.86	1.69–27.83	1.97–26.02	1.97–28.06	1.71–25.05
Index range	$-48 \leqslant h \leqslant 49$	$-20 \leqslant h \leqslant 25$	$-11 \leqslant h \leqslant 12$	$-12 \leqslant h \leqslant 13$	$-14 \leqslant h \leqslant 13$
	$-11 \leqslant k \leqslant 11$	$-22 \leqslant k \leqslant 17$	$-11 \leqslant k \leqslant 13$	$-12 \leqslant k \leqslant 13$	$0 \leqslant k \leqslant 16$
	$-33 \leqslant l \leqslant 23$	$-20 \leqslant l \leqslant 19$	$0 \leqslant l \leqslant 13$	$0 \leqslant l \leqslant 14$	$0 \leqslant l \leqslant 26$
Data, R_{int}, Parameters,	7697, 0.043, 452	8378, 0.018, 536	5232, 0.058, 280	4558, 0.029, 280	6490, 0.073, 416
R_1[a], wR_2[b] $[F^2 > 2\sigma(F^2)]$	0.042, 0.062	0.031, 0.092	0.044, 0.120	0.044, 0.116	0.054, 0.072
R_1[a], wR_2[b] [all data]	0.079, 0.069	0.046, 0.102	0.046, 0.125	0.045, 0.117	0.181, 0.103
Maximum and minimum peaks (e Å^{-3})	1.23, −0.50	1.10, −0.78	1.14, −0.68	1.32, −0.72	0.80, −0.62

[a] $R_1 : \sum ||F_o| - |F_c|| / \sum |F_o|$.
[b] $wR_2 : [\sum[w(F_o^2 - F_c^2)^2] / \sum[w(F_o^2)^2]]^{1/2}$.

Table 2
Selected bond lengths (Å) for **1**, **2**, **3**, **4** and **5**

1: GdBPA	
Gd–O(2C)#1	2.332(3)
Gd–O(1C)	2.360(3)
Gd–O(2B)#1	2.373(3)
Gd–O(2W)	2.423(3)
Gd–O(1W)	2.436(3)
Gd–O(1A)	2.447(3)
Gd–O(2A)	2.471(3)
Gd–O(1B)	2.481(3)
Gd–O(2B)	2.634(3)
Gd–Gd#1	3.9917(5)
2: HoBPA	
Ho(1)–O(2G)	2.322(9)
Ho(1)–O(1E)	2.321(9)
Ho(1)–O(2B)#2	2.334(10)
Ho(1)–O(1F)	2.421(11)
Ho(1)–O(2A)	2.429(8)
Ho(1)–O(2F)	2.437(10)
Ho(1)–O(1A)	2.432(11)
Ho(1)–O(1C)	2.486(9)
Ho(1)–O(2C)	2.534(9)
Ho(1)–C(1F)	2.796(15)
Ho(1)–C(1A)	2.831(10)
Ho(1)–C(1C)	2.847(9)
Ho(2)–O(1G)	2.278(10)
Ho(2)–O(2C)	2.355(9)
Ho(2)–O(1A)#3	2.364(12)
Ho(2)–O(2E)	2.382(16)
Ho(2)–O(1B)	2.398(7)
Ho(2)–O(2D)	2.417(10)
Ho(2)–O(1D)	2.432(11)
Ho(2)–O(2B)	2.483(11)
Ho(2)–O(1E)	2.591(9)
Ho(2)–C(1D)	2.788(9)
Ho(2)–C(1B)	2.810(9)
Ho(2)–C(1E)	2.878(10)
3: GdBIPY	
Gd–O(2B)#4	2.340(4)
Gd–O(2C)	2.364(5)
Gd–O(1C)#4	2.377(5)
Gd–O(2A)	2.442(5)
Gd–O(1B)	2.454(5)
Gd–O(1A)	2.484(5)
Gd–N(1)	2.581(6)
Gd–O(2B)	2.583(4)
Gd–N(2)	2.584(6)
Gd–Gd#4	3.9363(7)
4: HoBIPY	
Ho–O(2B)#4	2.329(4)
Ho–O(2C)	2.309(4)
Ho–O(1C)#4	2.352(5)
Ho–O(2A)	2.405(5)
Ho–O(1B)	2.419(5)
Ho–O(1A)	2.471(5)
Ho–O(2B)	2.577(5)
Ho–N(1)	2.554(5)
Ho–N(2)	2.574(5)
Ho–Ho#4	3.9165(9)
5: NdCrot	
Nd(1)–O(1D)	2.455(9)
Nd(1)–O(1W)	2.466(7)
Nd(1)–O(3W)	2.484(8)
Nd(1)–O(2W)	2.484(9)
Nd(1)–O(1C)#5	2.484(10)
Nd(1)–O(2A)	2.495(10)
Nd(1)–O(1B)	2.543(9)
Nd(1)–O(1A)	2.546(8)
Nd(1)–O(2B)	2.552(8)
Nd(2)–O(2D)	2.471(9)
Nd(2)–O(1A)#6	2.495(10)
Nd(2)–O(2C)	2.505(9)
Nd(2)–O(1E)	2.505(8)
Nd(2)–O(2F)	2.522(9)
Nd(2)–O(2B)	2.524(8)
Nd(2)–O(1F)	2.563(8)
Nd(2)–O(2E)	2.603(9)
Nd(2)–O(1C)	2.681(9)
Nd(2)–O(1D)	2.688(8)

Symmetry codes: #1 $-x+1/2,-y+1/2,-z+1$; #2 $x,-y+1,z+1/2$; #3 $x,-y+1,z-1/2$; #4 $-x,-y+2,-z+1$; #5 $-x+1,y+1/2,-z+1/2$; #6 $-x+1,y-1/2,-z+1/2$.

with the computer programs SHELXS-97 and SHELXL-97 [9], and SHELXTL-PC [10]. Full use of the CCDC package was also made for searching in the CSD Database [11].

Pertinent results are given in Tables 1–3, and Figs. 1–8, respectively.

2.3. Magnetic susceptibility measurements

Magnetic susceptibility data were collected in the temperature range 5–300 K on powdered samples, by using a SHE-906 SQUID susceptometer–magnetometer operated at 1 kG. The magnetic susceptibility data were corrected for the diamagnetism of the constituent atoms using Pascal's constants.

3. Results and discussion

3.1. Crystal structures

3.1.1. $[Gd_2(crot)_6(H_2O)_4]\cdot 4(bpa)$ (*1*)

The structure consists of $[Gd(crot)_3(aq)_2]_2$ dimers built up around a center of symmetry. The three independent crotonato molecules present in the structure show different coordination behaviors, viz., unit A is purely chelating, unit B is tridentate and unit C acts as a pure bridge. The bonds of two aqua molecules completes the usual nine coordination of gadolinium. The two cations in the dimer are thus connected by a quadruple bridge, two short Gd–O2B–Gd′ and two long Gd–O1C–C1C–O2C–Gd′, a situation which leads to an inter-cationic distance of 3.992(1) Å. Charge balance is achieved within the dimer, and so the two independent bpa solvate molecules are not protonated as it is the case of the Ho homologous (see below). The pyridyl groups in both bpa units present a *trans* disposition, and as result only one (N1) out of the two potentially active

Table 3
Hydrogen bonds **1** and **2** (Å and °)

D–H···A	*d*(D–H)	*d*(H···A)	*d*(D···A)	∠(DHA)
*Compound **1**:*				
N(2E)–H(2NE)···O(1A)	0.770(18)	2.209(19)	2.972(5)	171(4)
N(2D)–H(2ND)···O(1C)	0.771(18)	2.59(3)	3.204(6)	137(4)
O(1W)–H(1WB)···O(1B)#1	0.769(18)	2.115(19)	2.881(4)	174(5)
O(2W)–H(2WB)···N(1D)	0.777(18)	1.99(3)	2.738(6)	162(7)
O(2W)–H(2WA)···O(1W)	0.770(18)	2.53(5)	2.844(6)	107(4)
O(2W)–H(2WA)···O(1B)#1	0.770(18)	2.03(2)	2.796(5)	175(6)
O(1W)–H(1WA)···N(1E)	0.778(18)	2.02(2)	2.787(5)	166(5)
*Compound **2**:*				
N(1)–H(1N)···N(3)	1.32(11)	1.60(11)	2.494(17)	117(8)
N(2)–H(2B)···O(2F)	0.86(10)	1.80(11)	2.655(14)	173(7)

Symmetry codes: #1 $-x+1/2,-y+3/2,-z+1$.

unprotonated nitrogens (N1, N3) is able to interact with the core, acting as an acceptor for H-bonding, the remaining one pointing passively inwards. From the two amino protons, only the one attached to N2E makes a strong interaction to the chelating crotonato A, the other one being inhibited by steric reasons. The whole ensemble is shown in Fig. 1. These groups interact with each other through O1B, which is acceptor of two independent hydrogen bonds (suggested by the dashed lines in the packing diagram, Fig. 2) thus configuring a sort of H-bonded chains running along the very short unique *b*-axis. These chains, of which there are four in the unit cell, interact with each other rather weakly, mainly through van der Waals interactions.

3.1.2. $[Ho_2(crot)_7]_n\cdot(Hbpa)$ (**2**)

The main structure consists of chains of general formula $[Ho_2(crot)_7]_n$, evolving along the crystallographic *c*-axis, at approximate positions (x,y): $(0.90,0.0)$ and $(0.40,0.50)$. The elemental dinuclear unit conforming the chains is shown in detail in Fig. 3, while Fig. 4 displays a schematic view of the way in which the chains are formed. Inspection of both figures shows that there is a purely bridging crotonate (unit G), two purely chelating (units D and F) and four tridentate (units A, B, C and E) ones. As a result, both cations are ninefold coordinated, and linked to each other through two different types of links: one of them defined just by a double Ho1–O–Ho2 bridge (O: O1A, O2B) leading to an inter-cationic separation of 4.037(1) Å, and a second one showing a similar environment of a double Ho1–O–Ho2 bridge (O: O1E, O2C) plus a longer Ho1–O2G–C1G–O1G–Ho2 (through a whole carboxylate), leading to an almost identical Ho···Ho distance of 4.032(1) Å. The tails of the crotonate anions protrude outwards the chains, in two different orientations at right angles to each other, somehow resembling a cross in projection. This particular geometry leaves an empty space which upon packing forms channels parallel to the chain directions, in turn occupied by two hydration water molecules disordered into three main independent sites (occupations 0.80, 0.72 and 0.48) and the protonated bpa^{1+} acting as a counterion. The latter provides for the required charge balance, as the elemental units in the chains are negatively charged. In the intramolecular H-bond which builds up in the bpa^{1+} unit, the extra proton appears rather far away (1.32(11) Å) from its donor N1 and quite near to its acceptor N3 (1.60(11) Å), for which the usual D–H···A scheme for a classical interactions seems to drift towards something like D···H···D′. Similar situations could be traced in other bpa^{1+} anions in the literature [12–14].

Both the solvate and the counterion molecules are firmly attached to the columnar structure though H-bonding interactions, of which those corresponding to the hydration water can only be guessed through some very short O···O distances (since their H atoms could not be found) viz., O1W···O1F$[x-1,-y,z+1/2]$: 2.87 Å, O1W···O3W$[x-1/2,-y+3/2,z+1/2]$: 2.90 Å, O2W ··· O2A$[x,-y,z+1/2]$: 2.78 Å, O2W··· O1B $[x,-y, z+1/2]$: 2.75 Å, O3W···O2D$[x,-y,z+1/2]$: 3.11 Å and O3W···O1W$[x+1/2,y+3/2,z-1/2]$: 2.89 Å. The one involving the amino hydrogen in bpa, instead, can be fully characterized as a strong interaction: N2–H2A···O2F, H···O: 1.80(11)Å, O–H···O: 173(7)°. Fig. 5 gives a perspective view along the crystallographic *c* axis, where the way in which the molecules assemble can be clearly seen.

3.1.3. $[Gd_2(crot)_6(bipy)_2]$ (**3**), and $[Ho_2(crot)_6(bipy)_2]$ (**4**)

Compounds **3** and **4**, formulated as $[Ln(Crot)_3(bpy)]_2$ (Ln:Gd,Ho), are isostructural and will be described together. They organize as dimers built up around a symmetry center (Fig. 6), and each cation is coordinated to three crotonato groups binding in dissimilar coordination modes (unit A, purely chelating; unit B, tridentate; unit C, purely bridging). There is in addition a bipy unit, also chelating the cations through both nitrogens and protruding outwards at both sides of the dimer. This scheme results in a 10-fold coordi-

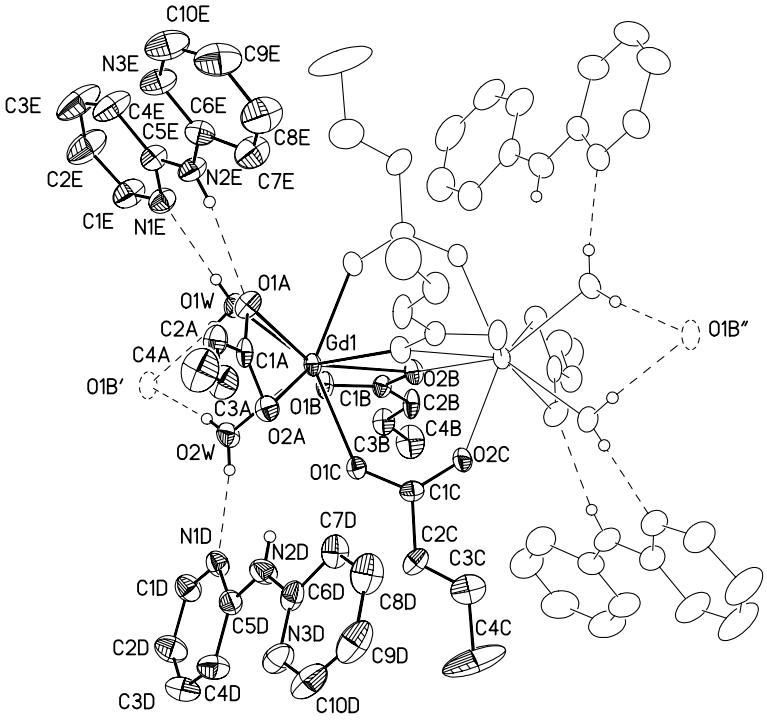

Fig. 1. Molecular diagram (XP in SHELXL, 1994) of the dimeric unit in **1**. Displacement ellipsoids drawn at 30% level. In dashed lines, the interactions leading to the formation of chains along *b*.

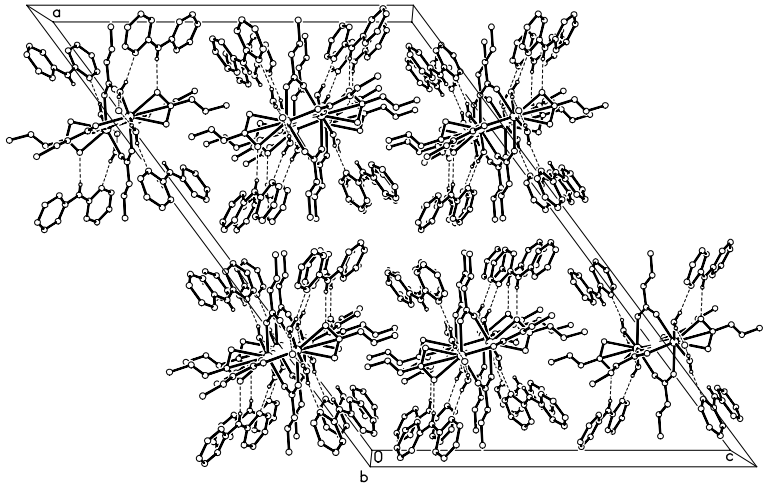

Fig. 2. Schematic diagram of the packing in **1** showing the way in which bpa molecules attach to the dimers. The H-bonded chains are shown in projection, coming out of the paper.

nation for the Ln cations, linked to each other through a quadruple bridge, two of them of the Ln–O–Ln type and two via a complete carboxylate, in a Ln–O–C–O–Ln′ sequence. The resulting inter-cationic distances are 3.936(1) Å for Gd and 3.917(1) Å for Ho.

The dimeric entities are fairly isolated in space; bipy units being too far away from one another to show any type of π interaction. The main source for packing stabilization are van der Waals interactions.

*3.1.4. $[Nd_2(crot)_6(H_2O)_3]_n$ (**5**)*

The Nd structure consists of unidimensional arrays of general formula $[Nd_2(crot)_6(H_2O)_3]_n$ running along the crystallographic *b*-axis (Fig. 7). The elemental links of these chains consist, in turn, of a binuclear entity made up of two very dissimilar NdO_n ($n = 9$, 10) coordination polyhedra built up around two independent neodymium centers (Fig. 8) conformed by crotonato anions behaving either as purely bidentate (crotonato units E, F) or

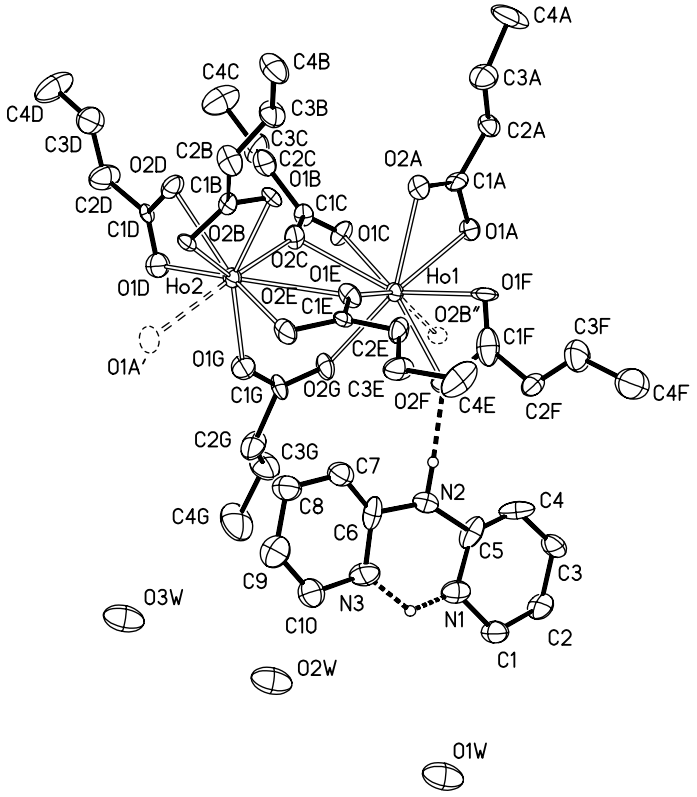

Fig. 3. Molecular diagram (XP in SHELXL, 1994) of the dimeric unit in **2**. Displacement ellipsoids drawn at 30% level.

tridentate (units A, B, C, D). Thus Nd1 gets four bonds from units A and B (providing two bonds each), another two from units C and D (one bond each) and three extra ones from the aqua molecules. Nd2, instead, which is only linked to carboxylates, receives four bonds from crotonates E and F (two bonds each), another four from units C and D (also two bonds each), and two bonds from A and B. This completes a nine-coordination scheme for Nd1 and a 10-coordination scheme for Nd2.

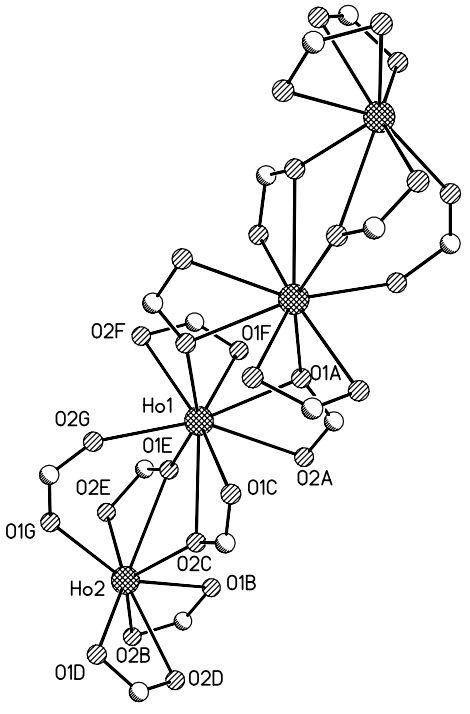

Fig. 4. Schematic view of the chains along the crystallographic *c*-axis in **2**.

This difference in coordination numbers shows up also in the Nd–O bond lengths, those to Nd1 being slightly shorter and with a smaller span than those to Nd2 (Nd1, span: 2.455(9)–2.552(8) Å, mean: 2.501(36) Å; Nd2, span: 2.471(9)–2.688(8) Å, mean: 2.555(77)). The neodymium centers are bridged in two different ways by two pairs of oxygens (O1D, O2B and O1C, O1A), thus defining two independent Nd1–O–Nd2–O rhomboidal loops giving rise to the chains. These are almost identical in size and shape, the Nd1···Nd2 distances being equal within experimental error (4.320(1) and 4.321(1) Å).

There is an uneven distribution of charges in the binuclear unit, the site at Nd1 being positively charged while the one at Nd2 is negative thus giving the ensemble a sort of zwiterion characteristic.

Although the quality of the data set impaired the possibility of finding the water hydrogens in a confident way, there are in the structure some 16O···OW distances shorter than 3.00 Å, amenable to result from hydrogen interactions, and thus suggesting a rather complex H-bonding scheme which provides both to the

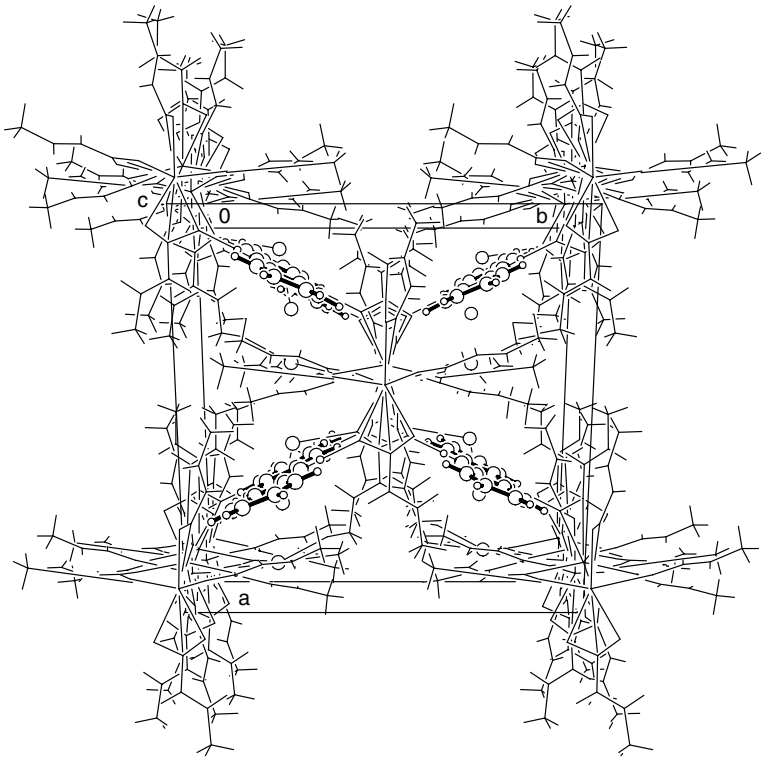

Fig. 5. Schematic diagram of the packing in **2**.

intra-chain cohesion, by means of the aqua molecules O1W to O3W, as well as to the packing stability through inter-chain interactions mainly mediated by the hydration water molecules O4W to (the disordered) O7W.

In comparing the schematic packing views of structures **2** and **5** some analogies are apparent in the way in which the 1D structures are formed. It is obvious how-

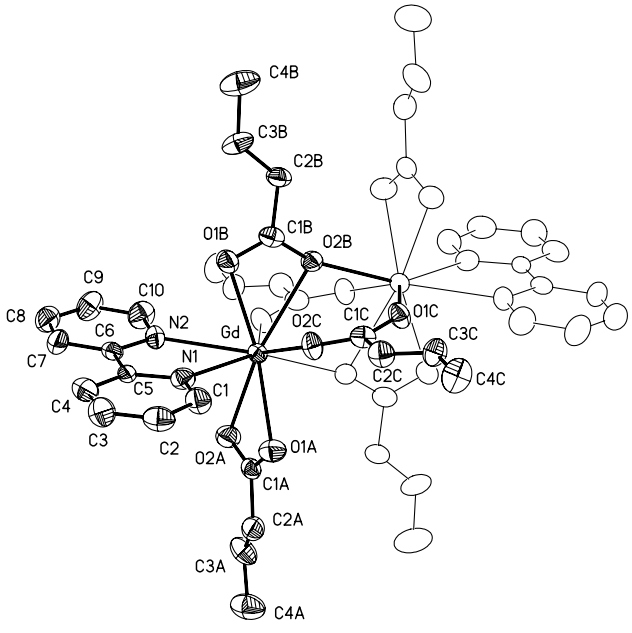

Fig. 6. Molecular diagram (XP in SHELXL, 1994) of the dimeric unit in **3**.

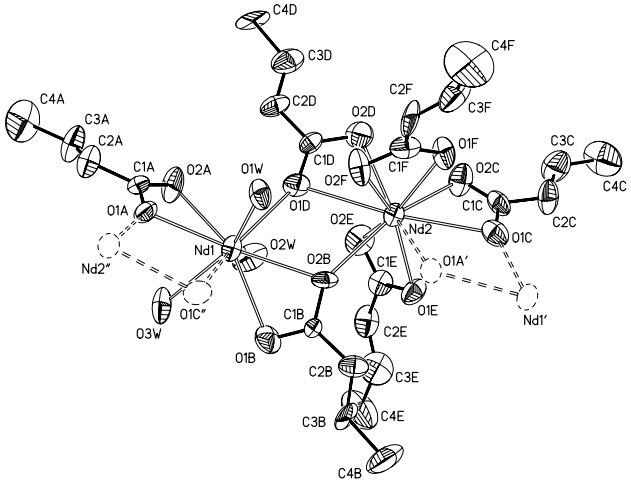

Fig. 7. Schematic view of the chains along the crystallographic *b*-axis in **5**.

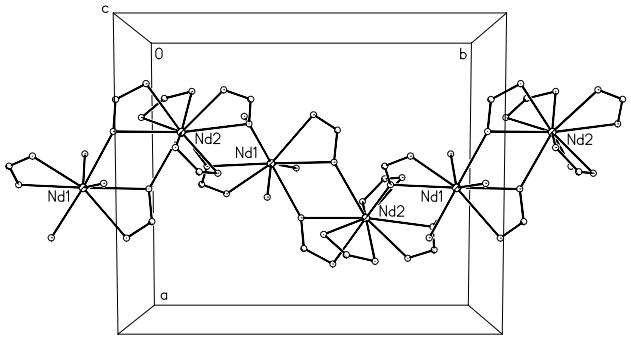

Fig. 8. Molecular diagram (XP in SHELXL, 1994) of the dimeric unit in **5**.

ever that the chains look rather different and this is due to the fact that in both structures the elemental rhomboidal links stack to each other in a different way: in the case of **2**, the best planes through contiguous links are almost normal to each other, subtending an angle of 95°, while in **5** the corresponding angle is just 45.2°. The second difference resides in the fact that the chains in **2** are "straighter" as measured by the angle subtended by adjacent Ln1···Ln2 segments: 23° in **2** against 44° in **5**, thus giving the latter their typical zig-zag look.

3.2. Magnetic properties

The study of magnetic properties of compounds **1**–**5** were performed through magnetic susceptibility measurements in the temperature range 5–300 K for compounds **1**, **3**, **5** and 2–300 K for compounds **2** and **4**. The temperature dependences of their magnetic susceptibility measured at 1 kOe are shown in Fig. 9, in the form of $1/\chi_m$ and $\chi_m T$ plots (χ_m, molar magnetic susceptibility and T, temperature).

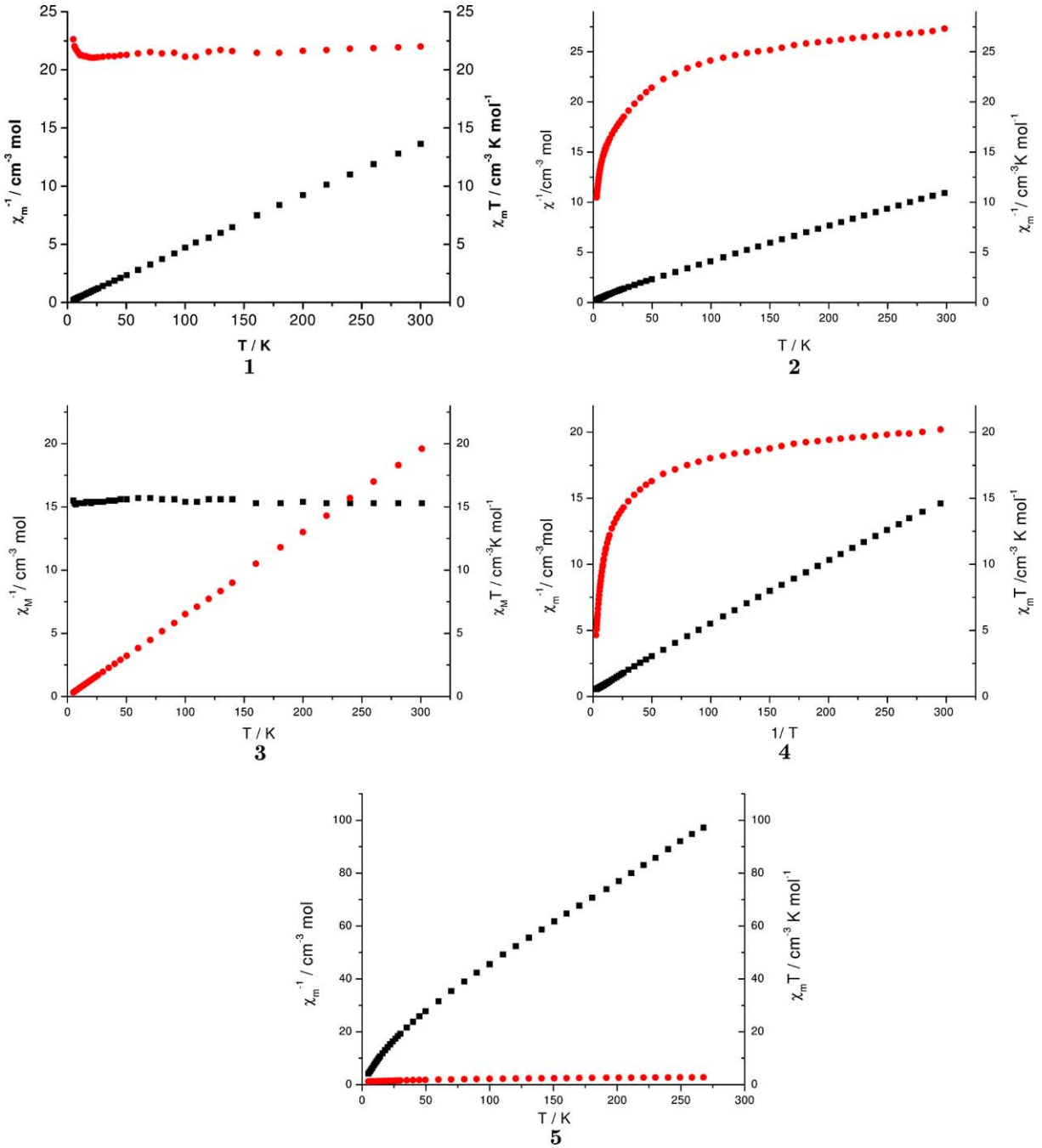

Fig. 9. Temperature dependence of the magnetic susceptibility and $\chi_m T$ of **1**, **2**, **3**, **4** and **5** complexes.

3.3. Gd complexes

Gd(III) presents a $4f^7$ electron configuration, with no orbital degeneracy. The $^8S_{7/2}$ ground term is located at some 30 000 cm^{-1} below the first excited state, leading to a magnetic moment corresponding to the spin-only value ion ($\mu_{eff} = g_J[J(J+1)]^{1/2} = 7.94$ MB per Gd(III)) independent of ligand field effects.

Complexes **1** and **3** show very similar magnetic behaviors, their $1/\chi_m$ plots obeying the Curie–Weiss law ($\chi_m(T) = C/T - \theta$) all through the investigated temperature range.

The curve fit for **1** yielded parameters $C = 21.8$ $cm^{-3}\,mol^{-1}\,K$, $\theta = -0.97$ K. The low negative value obtained for θ implies a weak antiferromagnetic interaction in this Gd(III) complex in agreement with an essentially constant $\chi_m T$ product as a function of temperature. The $\chi_m T$ value is practically constant in the 300–7 K range. The mean value of $\chi_m T$ is 21.71 $cm^{-3}\,mol^{-1}\,K$ allows us to calculate a magnetic moment of 9.25 MB, but slight increase in $\chi_m T$ is observed at 5 K ($\chi_m T = 22.62$ $cm^{-3}\,mol^{-1}\,K$, $\mu_{eff} = 9.48$ MB). The experimental magnetic moment derived from these fits was equal to 9.25 MB per gadolinium ion, somewhat larger than the expected value of 7.94 MB for Gd(III) in free-ion ground state ($C = 15.76$ $cm^{-3}\,mol^{-1}\,K$ for a dimeric unit).

Complex **3** displays an identical magnetic behavior with a constant $\chi_m T$ product in the investigated temperature range, with a magnetic moment of 7.8 MB per gadolinium ion calculated. The values for the constants C and θ are 15.33 $cm^{-3}\,mol^{-1}\,K$ and −0.4 K, respectively.

3.4. Ho complexes

The Ho(III) ion has a f^{10} configuration, with the $^5I_8$ ground term. The expected magnetic moment for a free-ion Ho(III) equals to 10.6 MB ($C = 28.09$ $cm^{-3}\,mol^{-1}\,K$) for a dimeric unit. In this compounds, the thermal population of the Stark components of Ho(III) dominates the magnetic properties.

Fig. 9 shows that for both Holmium complexes the low temperature $1/\chi_m$ vs T plots have negative intercepts with Weiss constant, $\theta = -12.9$ K for **2** and $\theta = -11.64$ K for **4**.

Similarly, the $\chi_m T$ plots show analogous behaviors, with values gradually decreasing with decreasing temperature. In the case of **2** $\chi_m T$ goes from 27.3 $cm^{-3}\,mol^{-1}\,K$ at 295 K down to 14.8 $cm^{-3}\,mol^{-1}\,K$ at 2.7 K which correspond to magnetic moment of 10.4 and 6.5 MB, respectively. The room temperature value $\mu_{eff} = 10.4$ MB per atom is very close to the expected value for two non-interacting holmium ion, 10.6 MB.

For the complex **4**, instead, $\chi_m T$ value span from 20.2 $cm^{-1}\,mol^{-1}\,K$ at 295 K, with a calculated magnetic moment of 9.92 MB down to 2.6 $cm^{-3}\,mol^{-1}\,K$ at low temperature, and a calculated moment of 43 MB.

3.5. Nd complex

Neodymium (III) has a $4f^3$ configuration with a $^4I_{9/2}$ free-ion ground state located some 2000 cm^{-1} below the first excited state $^4J_{11/2}$, fully depopulated even at room temperature.

Inspection of Fig. 9, shows that the experimental l magnetic values of complex **5** deviate from the Curie–Weiss law. The $\chi_m T$ vs T plot decreases gradually with decreasing temperature. At room temperature $\chi_m T$ is equal to 3.3 $cm^{-3}\,mol^{-1}\,K$ per atom which corresponds to a magnetic moment of 3.3 MB per neodymium atom, and very close to the value of the uncoupled $4f^3$ centers ($\mu = 3.62$ MB). On lowering the temperature down to 5 K this value decrease to 2.1 MB.

4. Discussion and conclusions

The synthetic studies in this work reveal that crotonic acid can behave as a versatile complexing agent with a potential ability to donate oxygen atoms to lanthanides, to which it can bind in a variety of coordination modes. We also conclude that the incorporation of diimines as ligands during the synthesis process can play a significant role in stabilizing the structures, both through their inclusion as a neutral ligand (compounds **1**, **3** and **4**), as a counterion (compound **2**) or just as an external crystallization agent (compound **5**).

In spite of the well-known ability of the carboxylato group to transmit magnetic interactions [7], the magnetic moments in the Gd complexes **1** and **3** are close to the calculated one of the free ion, suggesting that there are no magnetic interactions between the two crotonato-bridged metal centers in these binuclear complexes. This paramagnetic behavior is probably due to the Gd(III) centers being much apart and contrasts with the behavior reported in the literature for this type of compounds, which usually present antiferromagnetic interactions. To our knowledge, there are three examples in which the complexes shows an unexpected ferromagnetic exchange: one of these corresponds to a dimeric compound $[GdL_3H_2O]_2$ with $J = 0.05$ cm^{-1}, the second is a chain structure $[Gd(H_2L)(HL)(L)H_2O]_n$ with $J = 0.037$ cm^{-1}, (L = salicylato), reported by Costes et al. [15,16], and the third one correspond to the complex $[Gd(OAc)_3(H_2O)_2]_2 \cdot 4H_2O$ reported by Hatscher and Urland [17], that has a J value of 0.03 cm^{-1}.

In the Nd and Ho complexes, the deviation of the magnetic behavior from a Curie–Weiss law and the decrease of the $\chi_m T$ product can be attributed mainly to crystal field effects, which splits the free-ion ground state. A similar situation has been observed in the

monomeric $[NdL_2(H_2O)_4]ClO_4 \cdot 4H_2O$ complex with L = 2-formyl-4-methyl-(6-(*N*-2-pyridylethyl)formimidoyl)phenol reported by Kahn et al. [18], with a magnetic moment $\mu = 3.64$ MB at 300 K and $\mu = 2.54$ MB4 at 2 K. The smaller magnetic moment exhibited at low temperature in all complexes reported here (excepted Gd) are due to such crystal field effects.

4.1. Supplementary material

Crystallographic data for the structural analysis have been deposited with the Cambridge Crystallographic Data Centre, CCDC No. 205764–205768. For $[Gd_2(crot)_6(H_2O)_4] \cdot 4(bpa)$ (**1**); $[Ho_2(crot)_7]_n \cdot (Hbpa)$ (**2**); $[Gd_2(crot)_6(bipy)_2]$ (**3**); $[Ho_2(crot)_6(bipy)_2]$ (**4**) and $[Nd_2(crot)_6(H_2O)_3]_n$ (**5**), respectively. Copies of this information can be obtained free of charge from The Director, CCDC, 12 Union Road, Cambridge CB2 1EZ, UK, (Fax: +44-1223-336033, E-mail: linstead@ccdc.cam.ac.uk; or deposit@ccdc.cam.ac.uk).

Acknowledgements

The authors thank funding by FONDECYT (project 1020802), FONDAP (project 11980002), Fundación Andes (Project C-13575) and CNRS_CONICYT program PICS 922. J.C.M. is a grateful recipient of a Deutsdier Akademischer Austauschdient scholarship.

References

[1] C.H. Evans, Biochemistry of Lanthanides, Phenum, New York, 1990, p. 47.
[2] I.A. Setyawati, S. Liu, S.J. Retting, C. Orvig, Inorg. Chem. 39 (2000) 496.
[3] R.B. Lauffer, Chem. Rev. 87 (1987) 901.
[4] F.A. Hart, in: G. Wilkinson, R.D. Gillard, J.A. Mc Cleverty (Eds.), Comprehensive Coordination Chemistry, vol. 3, Pergamon Oxford, England, 1987, p. 1059.
[5] J. Rammo, H.J. Schneider, Leibigs Ann. (1996) 1756.
[6] S. Liu, L. Gelmiri, J. Steven, R.G. Rettig, R.C. Thompson, C. Orving, J. Am. Chem. Soc. 114 (1992) 6081.
[7] D.K. Towle, S.K. Hoffmann, W.E. Hatfield, P. Singh, P. Chaudhuri, Inorg. Chem. 27 (1988) 394.
[8] T. Yi, Song Gao, B. Li, Polyhedron 17 (13–14) (1998) 2243.
[9] G.M. Sheldrick, SHELXS-97 and SHELXL-97: Programs for Structure Resolution and Refinement, University of Göttingen, Germany, 1997.
[10] G.M. Sheldrick, SHELXTL-PC. version 5.0, Siemens Analytical X-ray Instruments, Inc., Madison, WI, 1994.
[11] F.H. Allen, O. Kennard, Chem. Des. Autom. News. 8 (1993) 131.
[12] F.A. Cotton, L.M. Daniels, G.T. Jordan, C.A. Murillo, Polyhedron 17 (1998) 589.
[13] S. Weng, Acta Crystallogr., Sect. C 54 (1998) 914.
[14] S.W. Ng, S.S.S. Raj, I.A. Razak, H.K. Fun, Main Group Metal Chem. 23 (2000) 193.
[15] J.P. Costes, J.M. Clemente-Juan, F. Dahan, F. Nicodéme, M. Verelst, Angew. Chem., Int. Ed. 41 (2) (2002) 323.
[16] J.P. Costes, J.M. Clemente-Juan, F. Dahan, F.J. Nicodéme, Chem. Soc., Dalton Trans. (2003) 1272.
[17] S.T. Hatscher, W. Urland, Angew. Chem., Int. Ed. 42 (2003) 2862.
[18] M. Andruh, E. Bakalbassis, O. Kahn, J.C. Trombe, P. Porcher, Inorg. Chem. 32 (1993) 1616.